HCFC2 is needed for IRF1- and IRF2-dependent *Tlr3* transcription and for survival during viral infections

Lei Sun,[1] Zhengfan Jiang,[3] Victoria A. Acosta-Rodriguez,[2] Michael Berger,[3] Xin Du,[3] Jin Huk Choi,[1] Jianhui Wang,[1] Kuan-wen Wang,[1] Gokhul K. Kilaru,[2] Jennifer A. Mohawk,[2] Jiexia Quan,[1] Lindsay Scott,[1] Sara Hildebrand,[1] Xiaohong Li,[1] Miao Tang,[1] Xiaoming Zhan,[1] Anne R. Murray,[1] Diantha La Vine,[1] Eva Marie Y. Moresco,[1] Joseph S. Takahashi,[2] and Bruce Beutler[1]

[1]Center for the Genetics of Host Defense and [2]Department of Neuroscience, Howard Hughes Medical Institute, University of Texas Southwestern Medical Center, Dallas, TX
[3]Department of Genetics, The Scripps Research Institute, La Jolla, CA

Transcriptional regulation of numerous interferon-regulated genes, including *Toll-like receptor 3* (*Tlr3*), which encodes an innate immune sensor of viral double-stranded RNA, depends on the interferon regulatory factor 1 (IRF1) and IRF2 transcription factors. We detected specific abrogation of macrophage responses to polyinosinic-polycytidylic acid (poly(I:C)) resulting from three independent *N*-ethyl-*N*-nitrosourea–induced mutations in *host cell factor C2* (*Hcfc2*). *Hcfc2* mutations compromised survival during influenza virus and herpes simplex virus 1 infections. HCFC2 promoted the binding of IRF1 and IRF2 to the *Tlr3* promoter, without which inflammatory cytokine and type I IFN responses to the double-stranded RNA analogue poly(I:C) are reduced in mouse macrophages. HCFC2 was also necessary for the transcription of a large subset of other IRF2-dependent interferon-regulated genes. Deleterious mutations of *Hcfc2* may therefore increase susceptibility to diverse infectious diseases.

INTRODUCTION

A sensor of double-stranded RNA (dsRNA), TLR3 mediates host defense against numerous viruses, including HSV-1 (Zhang et al., 2007), encephalomyocarditis virus (Hardarson et al., 2007; McCartney et al., 2011), respiratory syncytial virus (Rudd et al., 2005), hepatitis B virus (Karimi-Googheri and Arababadi, 2014), and influenza A virus (IAV; Le Goffic et al., 2006; Leung et al., 2014). Once activated, TLR3 signals via the adapter TRIF (TIR domain–containing adapter inducing IFN-β, also called TICAM-1), NF-κB, MAPKs, and IFN regulatory factor 3 (IRF3), leading to the production of proinflammatory cytokines and type I IFN (Yamamoto et al., 2002).

Tlr3 expression is itself regulated by type I and II IFNs, which drive a transcriptional program mediated by STAT and IRF transcription factors (Ivashkiv and Donlin, 2014; Schneider et al., 2014). TLR3 mRNA expression is regulated by IRF1, IRF2, and IRF8, which bind to at least one IRF element (IRF-E) in the *Tlr3* promoter to positively (IRF1 and IRF2) or negatively (IRF8) affect transcription (Heinz et al., 2003; Fragale et al., 2011). Both IRF1 and IRF2 are necessary for *Tlr3* transcription induced by IFN stimulation or viral infection, whereas only IRF2 is required for maintenance of the basal (unstimulated) level of *Tlr3* expression (Heinz et al., 2003; Nhu et al., 2006; Ren et al., 2015). By recruiting chromatin remodeling complexes such as BAF, IRF2 promotes an open chromatin state necessary for basal and induced *Tlr3* transcription (Ren et al., 2015). IRF1 is a strong activator of *Tlr3* transcription and is believed to compete with IRF2 for IRF-E binding after IFN stimulation (Ren et al., 2015).

At least nine IRF family members exhibit sequence and structural homology in their DNA-binding domains and therefore bind to similar IRF-E DNA sequences. The crystal structures of the DNA-binding domains of IRF1 or IRF2 in complex with a consensus IRF-E sequence showed that the IRFs induce DNA bending that may promote cooperative binding of additional IRFs and other transcription factors (Escalante et al., 1998; Fujii et al., 1999). However, little is known concerning the mechanisms by which IRFs discriminate between IRF-Es in different genes.

Using forward genetic analysis in mice, we discovered that HCFC2 is a critical component of the IRF1 and IRF2

Correspondence to Bruce Beutler: bruce.beutler@utsouthwestern.edu

Z. Jiang's present address is State Key Laboratory of Protein and Plant Gene Research and Key Laboratory of Cell Proliferation and Differentiation of the Ministry of Education, School of Life Sciences, Peking University, Beijing, China; and Peking-Tsinghua Center for Life Sciences, Beijing, China.

M. Berger's present address is Lautenberg Center for Immunology and Cancer Research, The Hebrew University of Jerusalem, Ein Kerem, Jerusalem, Israel.

X. Du's present address is COI Pharmaceuticals Inc., La Jolla, CA.

Abbreviations used: ChIP, chromatin immunoprecipitation; ChIP-seq, ChIP sequencing; dsRNA, double-stranded RNA; ENU, *N*-ethyl-*N*-nitrosourea; ERK, extracellular signal–regulated kinase; IAV, influenza A virus; IRF, IFN regulatory factor; IRF-E, IRF element; IRG, interferon-regulated gene; PM, peritoneal macrophage; poly(I:C), polyinosinic-polycytidylic acid; RNA-seq, RNA sequencing; TRIF, TIR domain–containing adapter inducing IFN-β.

The Rockefeller University Press
J. Exp. Med. 2017 Vol. 214 No. 11 3263–3277
https://doi.org/10.1084/jem.20161630

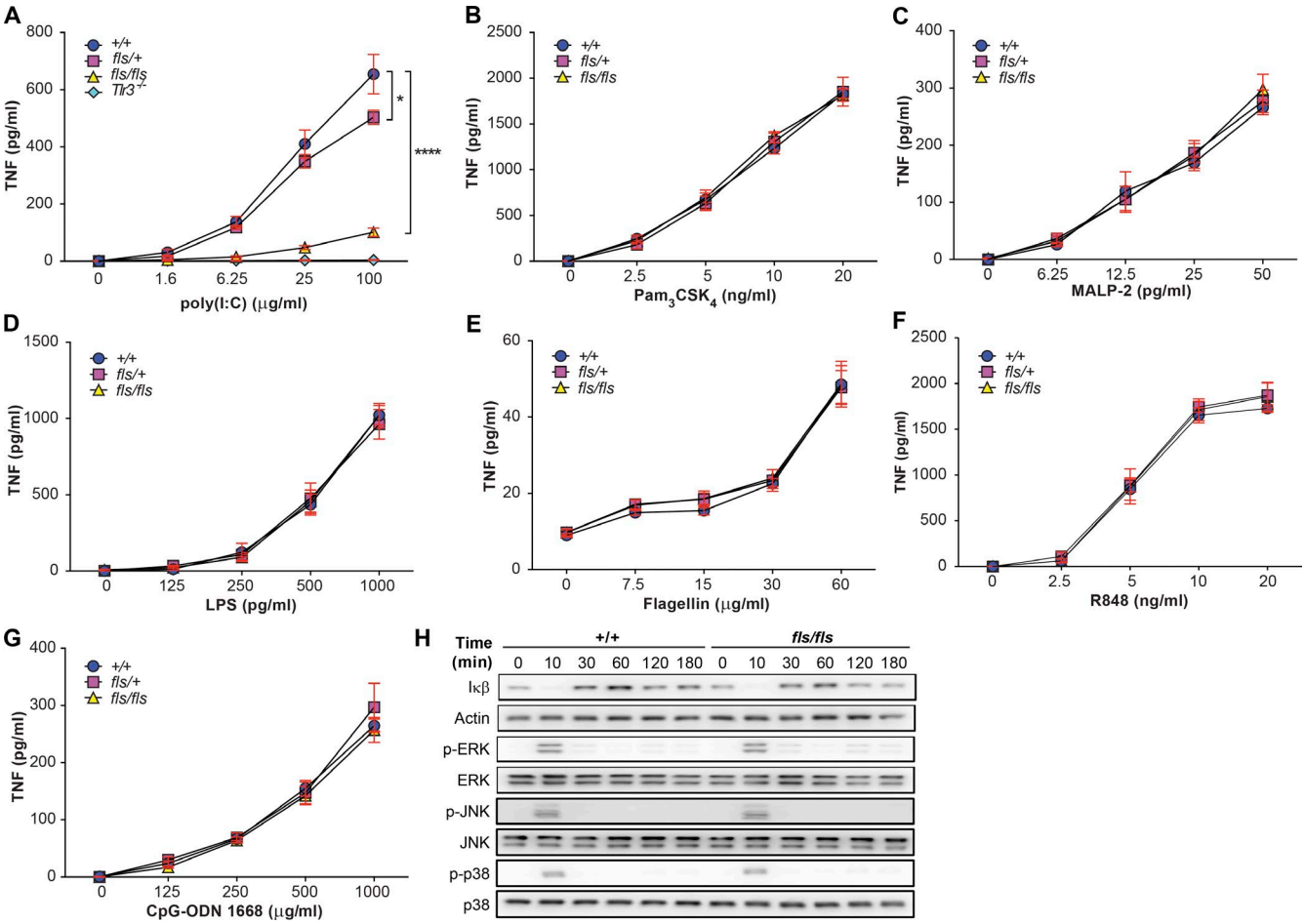

Figure 1. **Impaired responses to poly(I:C) of homozygous *fls* mice.** (A–G) PMs from WT (+/+), heterozygous *fls* (*fls*/+), and homozygous *fls* (*fls*/*fls*) mice were stimulated with poly(I:C) (TLR3 ligand; A), Pam_3CSK_4 (TLR2/1 ligand; B), macrophage-activating lipopeptide-2 (MALP-2; TLR2/6 ligand; C), LPS (TLR4 ligand; D), flagellin (TLR5 ligand; E), R848 (TLR7 ligand; F), and CpG-oligodeoxynucleotide 1668 (CpG-ODN; TLR9 ligand; G) in vitro at the indicated concentrations. TNF in the culture medium was measured by ELISA 4 h later. *Tlr3*$^{-/-}$ macrophages served as a negative control (A). *, $P \leq 0.05$; ****, $P \leq 0.0001$ (two-way ANOVA). Data represent mean ± SEM; $n = 4$ mice per genotype. (H) Immunoblot analysis of phosphorylated (p) ERK, p-JNK, p-p38, and the degradation of IκB at the indicated times after TNF treatment of PMs from *fls*/*fls* or WT mice. Total proteins and actin were used as loading controls. Results are representative of three independent experiments.

transcriptional machinery that regulates *Tlr3* and selected interferon-regulated gene (IRG) expression. The essential nature of HCFC2 is underscored by an increased susceptibility to viral infections in *Hcfc2*-deficient mice.

RESULTS

The *feckless* phenotype: Impaired TLR3 signaling

To identify genes involved in extracellular dsRNA sensing and signaling, we screened thioglycolate-elicited peritoneal macrophages (PMs) from third-generation descendants of *N*-ethyl-*N*-nitrosourea (ENU)–mutagenized C57BL/6J mice for TNF and IFN-β production in response to polyinosinic-polycytidylic acid (poly(I:C)). Short-term (4 h) treatment guaranteed that endosomal TLR3 signaling served as the major dsRNA sensory mechanism (Fig. 1 A).

A recessive phenotype with minor heterozygote effect, which we named *feckless* (*fls*) to denote a weak and ineffectual innate immune response, was characterized by reduced TNF production in response to poly(I:C) (Fig. 1 A). TNF production was normal in *fls* homozygous PMs in response to the TLR ligands Pam_3CSK_4 (TLR2/1), macrophage-activating lipopeptide-2 (TLR2/6), lipopolysaccharide (TLR4), flagellin (TLR5), R848 (TLR7), and CpG-oligodeoxynucleotide 1668 (TLR9; Fig. 1, B–G). In addition, TNF signaling remained intact (Fig. 1 H and Fig. S1). No other visible abnormalities were observed in homozygous *fls* mice.

A mutation of HCFC2

Genome-wide linkage analysis was performed to identify the mutation responsible for the *fls* phenotype (Xia et al., 2010).

A single linkage peak on distal chromosome 10 (logarithm of odds = 7.9527) established a 48.5-Mb critical region delimited by markers at 63,084,902 and 111,639,564 bp (Fig. 2 A). Whole-exome sequencing of DNA from an affected mouse identified a missense mutation within the critical region, a T-to-C transition at base pair 82,712,061 on chromosome 10. The mutation affects base pair 1,023 of the *Hcfc2* mRNA and results in a tryptophan-to-arginine substitution at amino acid 296 of HCFC2 (Fig. 2, B and C). Compound heterozygosity for the *Hcfc2*^{fls} allele and either of two other ENU-induced *Hcfc2* missense alleles (Fig. 2 C) reproduced the *fls* phenotype (Fig. 2 D). Moreover, homozygosity for a TALEN-mediated knockout allele of *Hcfc2* resulted in a more severe defect than observed in *fls* homozygotes, suggesting that the *fls* allele is hypomorphic (Fig. 2 E). These data confirmed that HCFC2 is necessary for the response to poly(I:C) in macrophages.

Immunoblot analysis of lysates of 3T3 fibroblasts expressing either WT HCFC2 or HCFC2^{fls} revealed reduced HCFC2^{fls} protein expression compared with WT HCFC2 (Fig. 2 F) despite comparable levels of transcript expression (Fig. 2 G), suggesting that the *fls* mutation causes protein instability and degradation.

Impaired TLR3 expression caused by HCFC2^{fls}

The defect of poly(I:C)-induced TNF production in *Hcfc2*$^{fls/fls}$ PMs suggested that TLR3-associated MAPK signaling, NF-κB signaling, or both might be disrupted. Homozygous *fls* PMs displayed reduced phosphorylation of p38, JNK, and extracellular signal–regulated kinase (ERK), and impaired IκB degradation in response to poly(I:C) treatment (Fig. 3 A), indicating that MAPK and NF-κB signaling is disrupted. Moreover, poly(I:C)-induced IFN-β production was impaired in *Hcfc2*$^{fls/fls}$ PMs (Fig. 3 B), as was phosphorylation of TBK1 (Fig. 3 A), indicating a defect of the IRF3-dependent pathway. IFN-β augments its own synthesis through an autoamplification loop involving JAK1, TYK2, and STAT1 (Darnell et al., 1994; Stark et al., 1998). In line with the observed reduction in IFN-β production, poly(I:C)-induced STAT1 phosphorylation was diminished in *Hcfc2*$^{fls/fls}$ PMs (Fig. 3 A). Thus, both the pathway leading to proinflammatory cytokine production and the pathway leading to type I IFN production were disrupted in homozygous *fls* PMs, indicating that TLR3 signaling was blocked either at the point of divergence of these two pathways (TRIF) or further upstream.

To test the effect of the *fls* mutation on TRIF function but without the possible confounding effect of a TLR3 defect, we examined LPS-induced signaling in *Myd88*$^{-/-}$ and *Myd88*$^{-/-}$*; Hcfc2*$^{fls/fls}$ PMs, which transduce TLR4 signals only through TRIF. PMs from *Myd88*$^{-/-}$ and *Myd88*$^{-/-}$*; Hcfc2*$^{fls/fls}$ mice displayed an equivalent magnitude and time course of ERK, p38, and STAT1 phosphorylation (Fig. 3 C), demonstrating that the *fls* mutation does not impair TRIF function. In addition to TRIF, TLR3 also recruits and activates phosphoinositide 3-kinase (PI3K) and its substrate, Akt, to fully activate IRF3 (Sarkar et al., 2004). Akt phosphorylation was abrogated in poly(I:C)-activated *Hcfc2*$^{fls/fls}$ PMs (Fig. 3 A).

TLR3 ligands must be brought into endosomes to interact with receptors, and the cell surface protein MSR1 facilitates uptake of poly(I:C) before delivery to endosomes (Limmon et al., 2008; DeWitte-Orr et al., 2010). Whereas TLR3 signaling in *Msr1*$^{-/-}$ PMs was rescued when the cationic liposomal transfection reagent DOTAP was used to artificially deliver poly(I:C) to endosomes, neither *Tlr3*$^{-/-}$ nor *Hcfc2*$^{fls/fls}$ PM responses were improved under the same conditions (Fig. 3 D), indicating that defective responses of *Hcfc2*$^{fls/fls}$ PMs were not due to impaired poly(I:C) uptake.

Because our data indicated a defect at the level of the TLR3 receptor caused by the HCFC2^{fls} mutation, we examined TLR3 mRNA and protein expression levels in HCFC2-deficient cells. We found that TLR3 protein was reduced in *Hcfc2*$^{fls/fls}$ PM lysates relative to WT PM lysates; both the endosomally cleaved functional form (Garcia-Cattaneo et al., 2012; Qi et al., 2012; Toscano et al., 2013) and the uncleaved form of TLR3 (trafficked from ER-Golgi) were affected (Fig. 3 E). We also found reduced transcript levels of *Tlr3* in unstimulated *Hcfc2*$^{fls/fls}$ PM lysates (Fig. 3 F). In *Hcfc2*$^{-/-}$ BMDMs, both basal and IFN-β–induced *Tlr3* transcription were significantly lower than in WT BMDMs, although the fold increase in *Tlr3* transcripts resulting from IFN-β treatment was similar between *Hcfc2*$^{-/-}$ and WT BMDMs (Fig. 3 G). These findings suggest that reduced TLR3 protein expression stems from impaired *Tlr3* transcription in macrophages lacking HCFC2. We conclude that defective TLR3 signaling in *Hcfc2*$^{fls/fls}$ macrophages is caused by inadequate amounts of TLR3.

HCFC2 facilitates IRF1/2 binding to the *Tlr3* promoter

HCFC1 binds to several transcription factors and chromatin modification enzymes via its β-propeller domain (Kristie et al., 1995; Wysocka and Herr, 2003), and we hypothesized that HCFC2 may bind and regulate the activity of transcription factors that control *Tlr3* expression. We used mass spectrometry of immunoprecipitated FLAG-tagged HCFC2 complexes to identify its interacting partners. Known interacting proteins, including histone-lysine *N*-methyltransferase SETD1A, retinoblastoma-binding protein 5 (RBBP5), and WD repeat-containing protein 5 (WDR5), were recovered in the HCFC2 precipitate, validating the experiment protocol (Table 1). We also identified IRF2 among the immunoprecipitated proteins (Table 1), and we tested the possible interaction between HCFC2 and either IRF2 or its closely related family member IRF1. We found that HCFC2 and IRF2 coimmunoprecipitated from 293T or THP-1 cell lysates (Fig. 4, A and B). Moreover, HCFC2 kelch-like repeats 5 and 6 within the β-propeller domain were minimally required for interaction with IRF2, while the IRF association domain of IRF2 was needed for binding to HCFC2 (Fig. S2). An association between HCFC2 and IRF1 was also detected (Fig. 4 A).

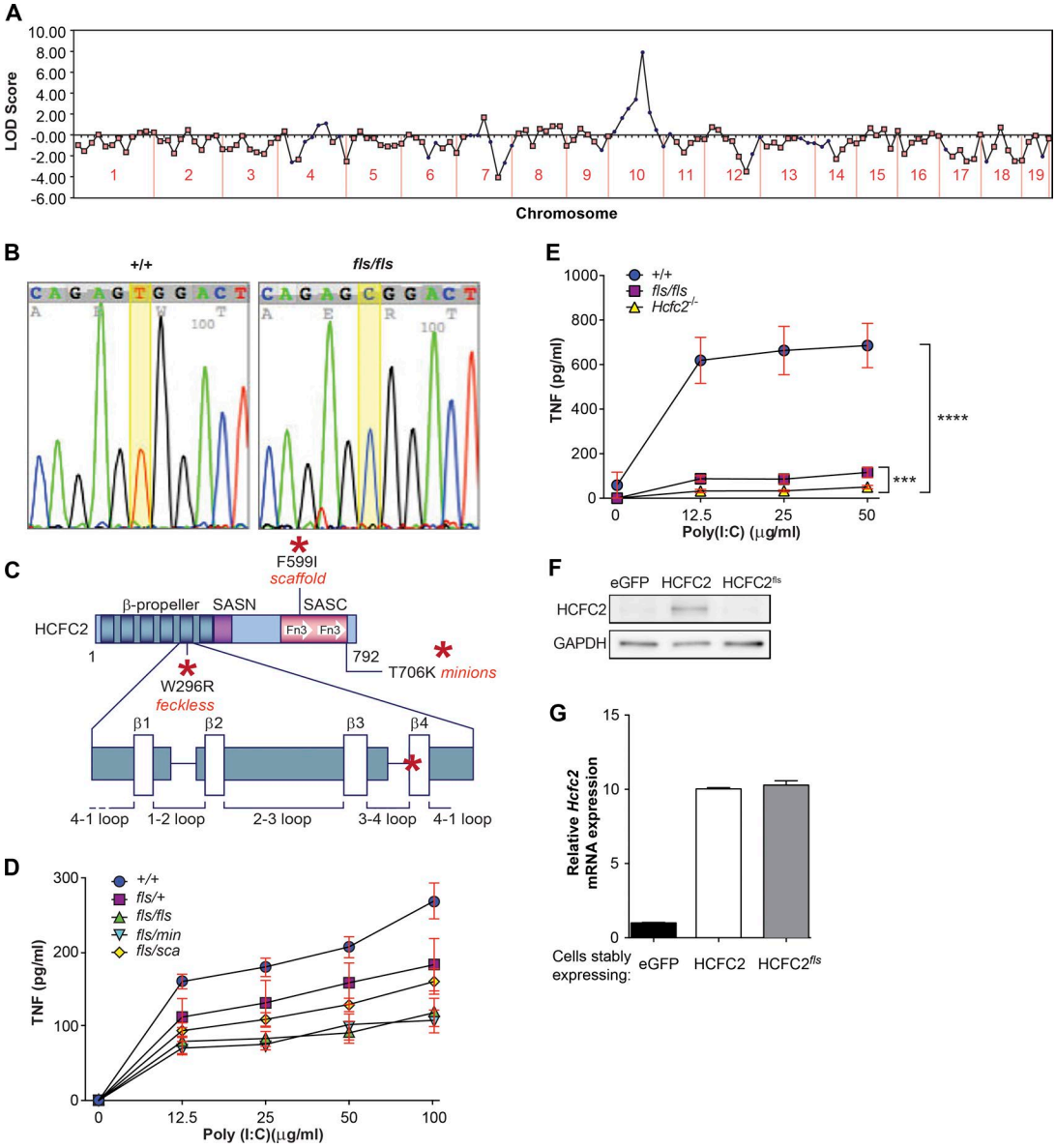

Figure 2. **The *fls* phenotype is caused by a mutation of *Hcfc2*.** (A) Chromosomal mapping of the *fls* mutation by bulk segregation analysis. Logarithm of odds (LOD) scores are shown for each chromosomal location. (B) DNA sequence chromatogram of *Hcfc2* in homozygous *fls* (*fls/fls*) or WT (+/+) mice in the region of the *fls* mutation. (C) Domain structure of HCFC2. The β-propeller domain contains six kelch-like repeats predicted to fold into a six-bladed β-propeller structure that mediates protein–protein interactions. There are two self-association domains of unknown function, one at the N terminus (SASN) and the other at the C terminus (SASC). The SASC domain has two tandem sequences with homology to fibronectin type 3 (Fn3) repeats. The *fls* mutation affecting amino acid 296 is within the fifth kelch repeat of HCFC2. The locations of the *scaffold* and *minions* mutations are also indicated. (D and E) TNF in the culture medium of PMs from age-matched heterozygous *fls* (*fls/+*), homozygous *fls* (*fls/fls*), compound heterozygous *fls/min*, compound heterozygous *fls/sca*, and WT (+/+) mice (D) or homozygous *fls* (*fls/fls*), TALEN-induced null *Hcfc2*$^{-/-}$, and WT (+/+) mice (E) stimulated with poly(I:C) for 4 h. $n = 3$ mice per genotype (D and E). ***, $P \leq 0.001$; **** $P \leq 0.0001$ (two-way ANOVA). (F and G) HCFC2 immunoblot analysis (F) and qRT-PCR measurement of *Hcfc2* mRNA normalized to *Gapdh* (G) in lysates of 3T3 cells stably transfected with plasmids expressing eGFP, WT HCFC2, or HCFC2^{fls}. Data represent mean ± SEM. Results are representative of two independent experiments.

We used gel shift experiments to test whether HCFC2 affects IRF1 or IRF2 binding to the *Tlr3* IRF-E. By itself, purified HCFC2 failed to bind a 28-bp DNA probe containing the IRF-E (Fig. 4 C, second lane), whereas shifted migration of the probe indicated formation of an IRF2/IRF-E complex (Fig. 4 C, third lane). Strikingly, increased IRF2/IRF-E complex formation was observed upon addition of HCFC2 to the reaction containing IRF2 and IRF-E DNA (Fig. 4 C, fourth lane); this complex was supershifted by an IRF2 antibody but not an HCFC2 antibody (Fig. 4,

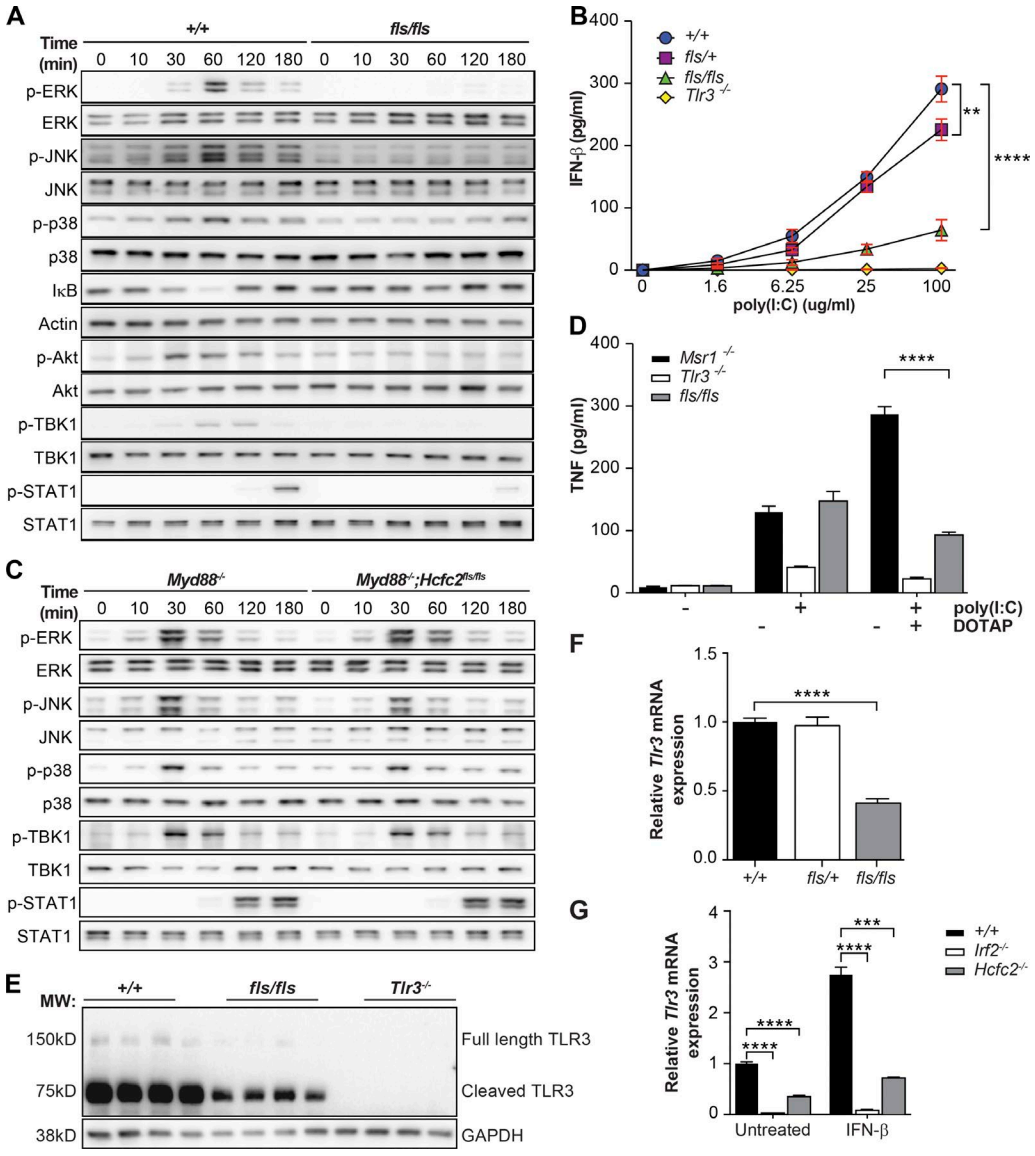

Figure 3. **Impaired TLR3 expression caused by HCFC2 mutation.** (A) Immunoblot analysis of phosphorylated (p) ERK, p-JNK, p-p38, p-Akt, p-TBK1, p-STAT1, and the degradation of IκB at the indicated times after poly(I:C) treatment of PMs from *fls/fls* or WT mice. Total proteins and actin were used as loading controls. (B) IFN-β in the culture medium of PMs from *fls* heterozygous, *fls* homozygous, or WT mice 4 h after treatment with poly(I:C) at the indicated concentrations. $Tlr3^{-/-}$ macrophages served as a negative control. (C) Immunoblot analysis of p-ERK, p-JNK, p-p38, p-TBK1, and p-STAT1 at the indicated times after LPS treatment of PMs from $Myd88^{-/-}$ or $Myd88^{-/-}Hcfc2^{fls/fls}$ mice. Total proteins were used as loading controls. (D) TNF in the culture medium of PMs from *fls* homozygous, $Msr1^{-/-}$, or $Tlr3^{-/-}$ mice 24 h after treatment with poly(I:C) with or without DOTAP. (E) Immunoblot analysis of full-length and cleaved TLR3 in PMs from WT (+/+), homozygous *fls* (*fls/fls*), and $Tlr3^{-/-}$ mice. (F) qRT-PCR measurement of *Tlr3* mRNA normalized to *Gapdh* in PMs from heterozygous *fls*, homozygous *fls*, and WT (+/+) littermates. Expression level was plotted relative to that in WT cells. (G) qRT-PCR measurement of *Tlr3* mRNA normalized to *Gapdh* in untreated or IFN-β-stimulated BMDMs from $Irf2^{-/-}$, $Hcfc2^{-/-}$, and WT (+/+) mice. Expression level was plotted relative to that in untreated WT cells. **, $P \leq 0.01$; ***, $P \leq 0.001$; ****, $P \leq 0.0001$, two-way ANOVA (B) or unpaired Student's *t* test (D, F, and G). Data represent mean ± SEM; *n* = 3 or 4 mice per genotype (B, D, F, and G). Results are representative of three independent experiments.

C [sixth and seventh lanes] and D), indicating that HCFC2 was not part of the IRF2/IRF-E complex. HCFC2 exerted a similar effect on the interaction between IRF1 and IRF-E DNA (Fig. 4 E). Consistent with these data, gel shift analysis performed using nuclear extracts of WT or $Hcfc2^{-/-}$ PMs demonstrated reduced IRF2/IRF-E complex formation by $Hcfc2^{-/-}$ extracts relative to WT extracts (Fig. 4 F). To provide further evidence, chromatin immunoprecipitation (ChIP) using an IRF2 antibody was performed and significantly reduced association between IRF2 and the IRF-E site in the *Tlr3* promoter was found in $Hcfc2^{-/-}$ MEFs compared with WT MEFs (Fig. 4 G).

In summary, the data in this section suggest that HCFC2 forms complexes with IRF2 and IRF1 to facilitate their binding to the *Tlr3* IRF-E and that HCFC2 releases these IRFs upon their binding to DNA.

Genome-wide analysis of gene regulation by IRF2 and HCFC2

IRF1 and IRF2 regulate the transcription of numerous IRGs in addition to *Tlr3*. To investigate whether HCFC2 may be important for IRF2 transcriptional regulation of genes other than *Tlr3*, ChIP sequencing (ChIP-seq) was conducted using an IRF2 antibody and either WT or *Hcfc2*$^{-/-}$ MEFs (Fig. 5 A). A total of 6,369 DNA-binding sites for IRF2 were identified in WT and *Hcfc2*$^{-/-}$ samples combined (Tables S1 and S2), and among them 381 were differentially enriched in either WT or *Hcfc2*$^{-/-}$ samples (Table S3): greater quantities of 365 (95.8%) DNA sequences were immunoprecipitated from WT MEFs relative to *Hcfc2*$^{-/-}$ MEFs (Fig. 5 B), whereas 16 (4.2%) sequences were increased in IRF2 immunoprecipitates from *Hcfc2*$^{-/-}$ MEFs relative to WT MEFs. Strikingly, motif analysis of the 365 binding sequences that were enriched in WT samples showed that 55.07% matched the consensus IRF2-binding site (Fig. 5 C; $P = 10^{-227}$); none of the 16 *Hcfc2*$^{-/-}$-enriched binding sequences matched the IRF2 consensus binding sequence. Analysis of the flanking regions found no significantly preferred sequence. These findings suggest that HCFC2 is necessary for the association of IRF2 with several of its targets.

As a complement to the ChIP-seq data, we performed RNA sequencing (RNA-seq) to examine the genome-wide transcriptional consequences of *Hcfc2* or *Irf2* deficiency in BMDMs. Pearson correlation coefficient analysis showed strong correlations between biological replicates in each group (Fig. 6 A). When normalized to WT BMDMs, *Hcfc2*$^{-/-}$ BMDMs showed significant changes of expression in 1,210 genes, and *Irf2*$^{-/-}$ showed significant changes of expression in 1,026 genes. Altogether, the expression of 571 genes was similarly altered (increased or decreased) in *Hcfc2*$^{-/-}$ and *Irf2*$^{-/-}$ BMDMs compared with WT BMDMs; these represent 47% (571 of 1,210) and 56% (571 of 1,026) of all genes affected by the respective mutations (Fig. 6, B and C). After IFN-β treatment, 71% (403 of 571) of the genes that were similarly affected by *Irf2* and *Hcfc2* mutations remained significantly differentially expressed, with both mutations resulting in the same direction of change relative to WT samples (Fig. 6 C).

Comparison of ChIP-seq and RNA-seq data revealed a total of 31 genes that showed both reduced association with IRF2 and altered transcript levels in *Hcfc2*$^{-/-}$ samples rela-

Table 1. **HCFC2-interacting proteins identified by mass spectrometry of immunoprecipitated Flag–HCFC2 complexes**

Protein description	Spectral counts		
	Flag–HCFC2	Control 1	Control 2
HNRH2_HUMAN Heterogeneous nuclear ribonucleoprotein H2 OS = *Homo sapiens* GN = HNRNPH2 PE = 1 SV = 1	94.00	9.00	7.00
SET1A_HUMAN Histone-lysine *N*-methyltransferase SETD1A OS = *Homo sapiens* GN = SETD1A PE = 1 SV = 3	47.08		
DIDO1_HUMAN Death-inducer obliterator 1 OS = *Homo sapiens* GN = DIDO1 PE = 1 SV = 5	31.88		1.00
CXXC1_HUMAN CpG-binding protein OS = *Homo sapiens* GN = CXXC1 PE = 1 SV = 2	27.78		
SIR1_HUMAN NAD-dependent protein deacetylase sirtuin-1 OS = *Homo sapiens* GN = SIRT1 PE = 1 SV = 2	25.86		
WDR5_HUMAN WD repeat-containing protein 5 OS = *Homo sapiens* GN = WDR5 PE = 1 SV = 1	22.00	2.00	
RBBP5_HUMAN Retinoblastoma-binding protein 5 OS = *Homo sapiens* GN = RBBP5 PE = 1 SV = 2	22.00		
BD1L1_HUMAN Biorientation of chromosomes in cell division protein 1–like 1 OS = *Homo sapiens* GN = BOD1L1 PE = 1 SV = 2	19.98		
F5H8F7_HUMAN Set1/Ash2 histone methyltransferase complex subunit ASH2 OS = *Homo sapiens* GN = ASH2L PE = 2 SV = 1	15.96	1.00	
ZHANG_HUMAN CREB/ATF bZIP transcription factor OS = *Homo sapiens* GN = CREBZF PE = 1 SV = 2	15.85	0.99	
ZN639_HUMAN Zinc finger protein 639 OS = *Homo sapiens* GN = ZNF639 PE = 1 SV = 1	12.92		
THA11_HUMAN THAP domain–containing protein 11 OS = *Homo sapiens* GN = THAP11 PE = 1 SV = 2	12.00		
ZBTB2_HUMAN Zinc finger and BTB domain-containing protein 2 OS = *Homo sapiens* GN = ZBTB2 PE = 1 SV = 1	11.00		
NUDC3_HUMAN NudC domain–containing protein 3 OS = *Homo sapiens* GN = NUDCD3 PE = 1 SV = 3	10.00		
THAP7_HUMAN THAP domain–containing protein 7 OS = *Homo sapiens* GN = THAP7 PE = 1 SV = 2	5.00		
F8W6N3_HUMAN Ubiquitin carboxyl-terminal hydrolase BAP1 OS = *Homo sapiens* GN = BAP1 PE = 2 SV = 1	5.00		
KDM4A_HUMAN Lysine-specific demethylase 4A OS = *Homo sapiens* GN = KDM4A PE = 1 SV = 2	5.00		
THAP9_HUMAN DNA transposase THAP9 OS = *Homo sapiens* GN = THAP9 PE = 1 SV = 2	5.00		
BACH1_HUMAN Transcription regulator protein BACH1 OS = *Homo sapiens* GN = BACH1 PE = 1 SV = 2	4.99		
SHOT1_HUMAN Shootin-1 OS = *Homo sapiens* GN = KIAA1598 PE = 1 SV = 4	4.95		
KMT2A_HUMAN Histone-lysine *N*-methyltransferase 2A OS = *Homo sapiens* GN = KMT2A PE = 1 SV = 5	4.00		
IF4A3_HUMAN Eukaryotic initiation factor 4A-III OS = *Homo sapiens* GN = EIF4A3 PE = 1 SV = 4	4.00		
IRF2_HUMAN Interferon regulatory factor 2 OS = *Homo sapiens* GN = IRF2 PE = 1 SV = 2	4.00		
F208B_HUMAN Protein FAM208B OS = *Homo sapiens* GN = FAM208B PE = 1 SV = 1	4.00		
B4DY82_HUMAN Sentrin-specific protease 5 OS = *Homo sapiens* GN = SENP5 PE = 2 SV = 1	3.00		
KMT2B_HUMAN Histone-lysine *N*-methyltransferase 2B OS = *Homo sapiens* GN = KMT2B PE = 1 SV = 1	3.00		
KHNYN_HUMAN Protein KHNYN OS = *Homo sapiens* GN = KHNYN PE = 2 SV = 3	3.00		
E7EN32_HUMAN Menin OS = *Homo sapiens* GN = MEN1 PE = 2 SV = 1	3.00		
J3QSB5_HUMAN 60S ribosomal protein L36 OS = *Homo sapiens* GN = RPL36 PE = 2 SV = 1	3.00		
CEP55_HUMAN Centrosomal protein of 55 kD OS = *Homo sapiens* GN = CEP55 PE = 1 SV = 3	3.00		

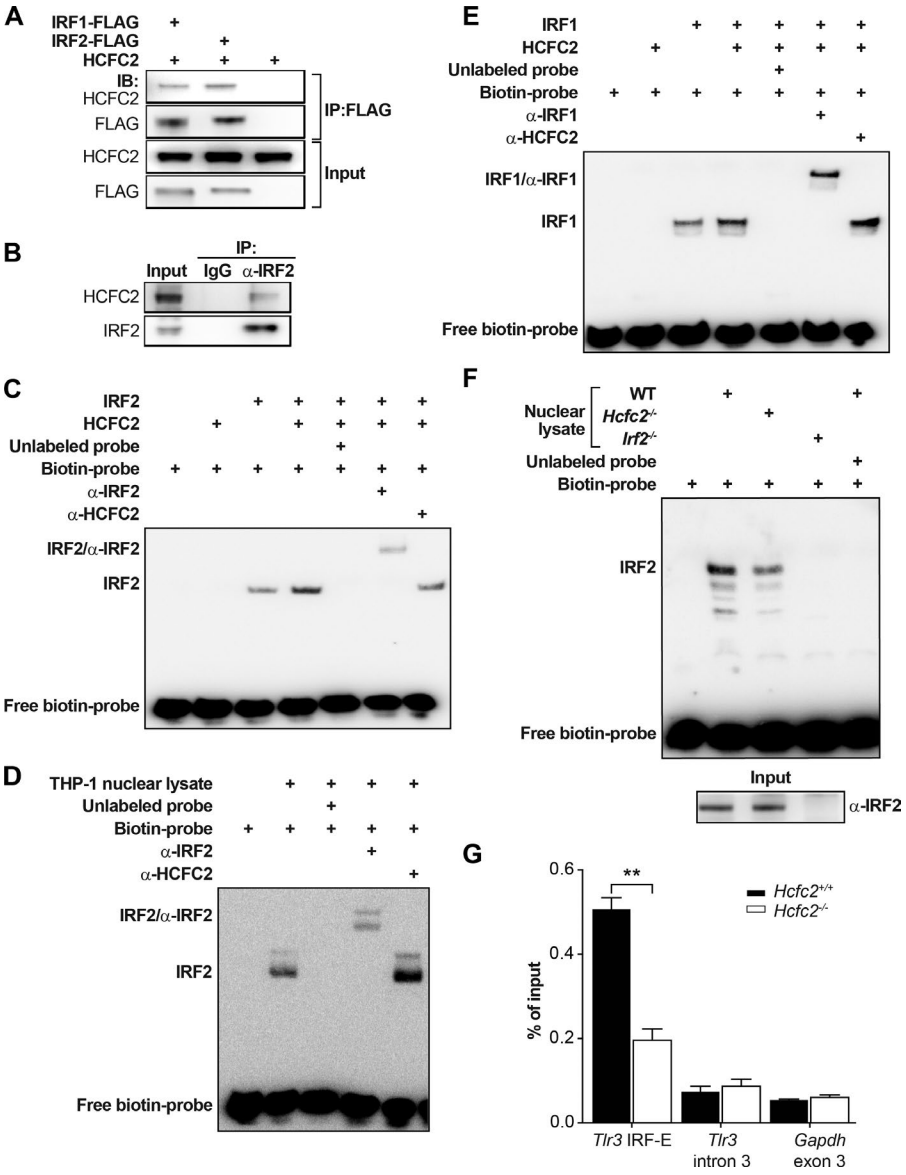

Figure 4. **HCFC2 binds to IRF2 and IRF1 to facilitate their binding to the *TLR3* IRF-E.** (A) Immunoprecipitation and immunoblot analysis of lysates of 293T cells transiently overexpressing FLAG-tagged IRF1 or IRF2 and HCFC2. (B) Immunoprecipitation and immunoblot analysis of endogenous HCFC2 and IRF2 in cross-linked nuclear extracts of THP-1 cells. (C) Gel shift analysis of the binding of purified human IRF2 and HCFC2 to a biotin-labeled 28-bp DNA probe containing the human *TLR3* IRF-E. (D) Gel shift analysis using nuclear lysates of THP-1 cells of the binding of endogenous IRF2 to a biotin-labeled 28-bp DNA probe containing the *TLR3* IRF-E. (E) Gel shift analysis of the binding of purified human IRF1 and HCFC2 to a biotin-labeled 28-bp DNA probe containing the human *TLR3* IRF-E. The positions of IRF/DNA and IRF/α-IRF/DNA complexes are indicated in C–E. (F top) Gel shift analysis using nuclear lysates of BMDMs from WT, *Hcfc2*$^{-/-}$, or *Irf2*$^{-/-}$ mice of the binding of endogenous IRF2 to a biotin-labeled 28-bp DNA probe containing the mouse *Tlr3* IRF-E. The position of the IRF2/DNA complex is indicated. (Bottom) IRF2 immunoblot of the input nuclear lysates used for gel shift analysis. (G) ChIP analysis of IRF2 binding to the *Tlr3* promoter in *Hcfc2*$^{+/+}$ and *Hcfc2*$^{-/-}$ MEFs. Sites within intron 3 of *Tlr3* and exon 3 of *Gapdh* served as negative controls. The results of the real-time PCR are graphed as a percentage of the input sample. **, $P \leq 0.01$ (unpaired Student's *t* test). Data represent mean ± SEM; $n = 3$ samples per group. Results are representative of two (D) and three (A–C and E–G) independent experiments.

tive to WT samples: 13 with significantly decreased mRNA expression and 18 with increased mRNA expression in *Hcfc2*$^{-/-}$ samples (Table 2). These results suggest that HCFC2 facilitates the binding of IRF2 to a variety of target genes to support the functions of IRF2 as both a transcriptional activator and a transcriptional repressor. Because different cell types were used in ChIP-seq and RNA-seq experiments, we note that the overlapping gene set may underestimate the true number of genes coregulated by HCFC2 and IRF2.

Defective host defense caused by *Hcfc2* deficiency

Among genes whose expression was affected by HCFC2 and IRF2 deficiencies, a substantial number are known IRGs or contain an IRF-E in their promoter regions. Indeed, IFN-β stimulation induced the transcription of 888 genes in WT BMDMs, among which 153, 132, or 72 genes showed reduced expression in *Irf2*$^{-/-}$ BMDMs, *Hcfc2*$^{-/-}$ BMDMs, or in both *Irf2*$^{-/-}$ and *Hcfc2*$^{-/-}$ BMDMs. The diminished expression of four IRGs in *Hcfc2*$^{-/-}$ and *Irf2*$^{-/-}$ BMDMs was confirmed by quantitative RT-PCR (qRT-PCR; Fig. 7, A–D). Notably, these four genes, *Trail* (TNF-related apoptosis-inducing ligand), *Iigp1* (interferon inducible GTPase 1), *Mov10* (Moloney leukemia virus 10), and *Ifi47* (IFN-γ-inducible protein 47), as well as other untested IRGs, are known immune response genes involved in defense against parasitic, bacterial, and viral infections, suggesting an important role of *Hcfc2* in host defense.

Indeed, when challenged with IAV, 100% of homozygous *fls* mice died by 12 d after infection; WT mice recovered from IAV infection by day 9 after infection (Fig. 7 E). No significant differences in weight loss were observed between the homozygous *fls* and WT mice after IAV infection (Fig. 7 F).

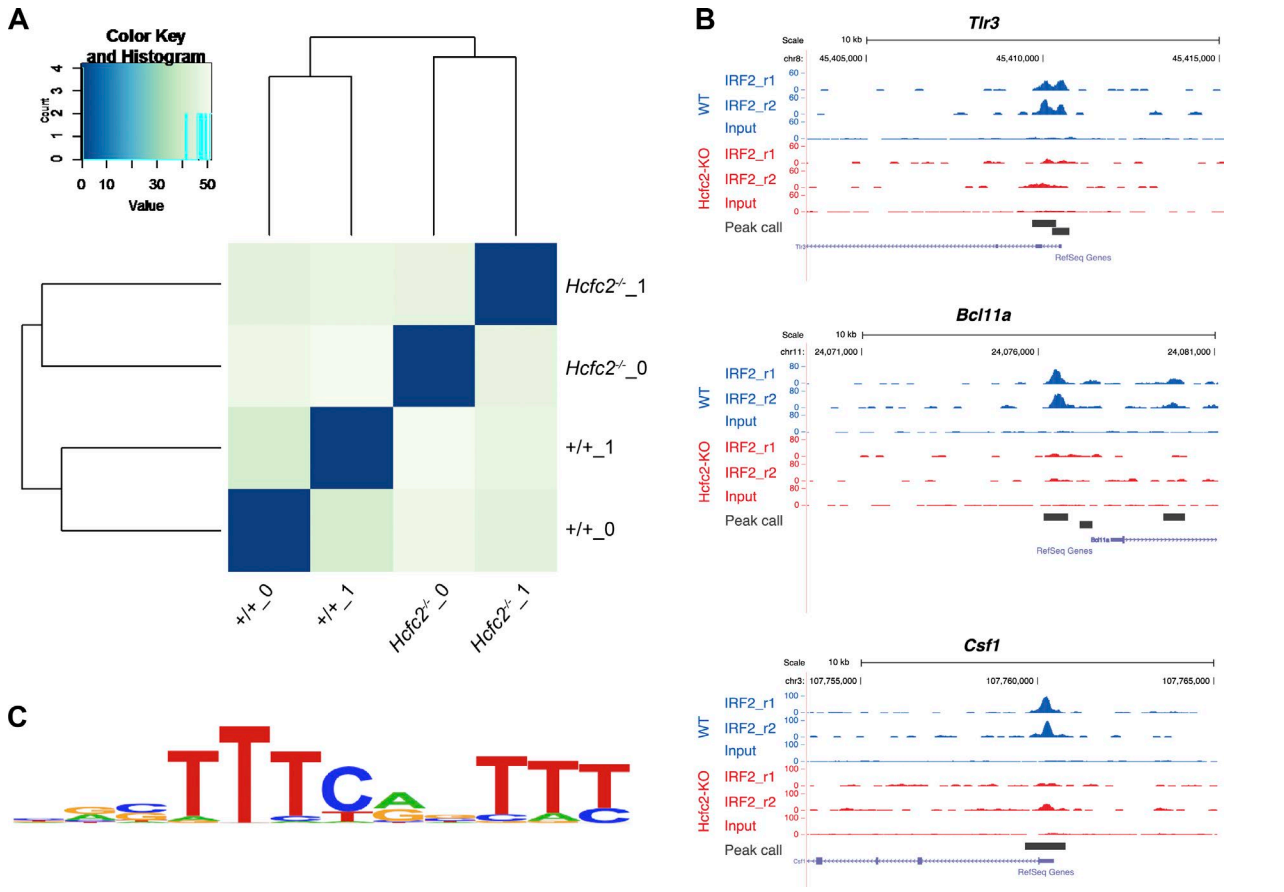

Figure 5. **HCFC2 facilitates IRF2 association with its DNA targets across the genome.** ChIP-seq analysis of IRF2-bound DNA precipitated from MEFs derived from *Hcfc2*$^{-/-}$ or WT (+/+) mice (n = 2 mice per genotype). (A) Complete linkage analysis of the biological replicates indicated similarity between the two *Hcfc2*$^{-/-}$ samples or the two WT samples was stronger than between either *Hcfc2*$^{-/-}$ sample and either WT sample. (B) University of California, Santa Cruz Genome Browser view of IRF2 binding peaks in WT or *Hcfc2*$^{-/-}$ MEFs for three representative target genes, *Tlr3*, *Bcl11a*, and *Csf1*. (C) The DNA sequence motif bound by IRF2 was determined by motif analysis of the 365 WT enriched DNA-binding sites. Letter height represents the frequency with which the nucleotide was present at that position in the bound DNA sequences. De novo sequence motif analysis was performed with ±100-bp DNA sequence from the master peak binding sites by HOMER. ChIP-seq experiment was performed one time.

Fls homozygotes infected with HSV1 developed ataxia and paralysis; all died within 5 d after infection, whereas infected WT mice survived past 8 d after infection (Fig. 7 G). In addition, HSV1-induced IFN-α and IFN-β were reduced in serum from infected homozygous *fls* mice compared with infected WT mice (Fig. 7, H and I). These data demonstrate that *fls* mutant mice display susceptibility to multiple virus infections and support that *Hcfc2* is required for proper host defense.

DISCUSSION

IRF1 and IRF2 regulate *Tlr3* transcription by binding to an IRF-E near the transcription start site of *Tlr3*. We found that HCFC2, a protein with previously unknown function, formed a complex with IRF1 or IRF2 and promoted their binding to the *Tlr3* IRF-E and to other gene targets. We hypothesize that the interaction between HCFC2 and either IRF1 or IRF2 may generate a conformational change in the IRF that favors DNA binding. An effect of amino acid substitutions or of protein interactions with the IRF2 C terminus, to which HCFC2 binds, on DNA binding by the N terminus has previously been reported (Childs and Goodbourn, 2003; Prakash and Rath, 2010) and supports this hypothesis. Moreover, a function similar to the one we propose for HCFC2 has been suggested for HCFC1 in its interaction with VP16, an HSV protein that directs the formation of a DNA-binding complex necessary for viral immediate early gene transcription (Kristie and Sharp, 1990). In that system, HCFC1 was required for the formation of a tripartite complex containing HCFC1, VP16, and Oct 1 that associated with viral DNA (Gerster and Roeder, 1988; Katan et al., 1990; Xiao and Capone, 1990). VP16 showed little DNA-binding activity by itself, but this activity was enhanced by a cycle of protein denaturation–partial renaturation or by formation of the VP16–Oct1–HCFC1 complex, both of which are suggestive of conformational change (Marsden et al., 1987; Kristie and Sharp, 1990). HCFC1 bound directly to VP16 in the absence

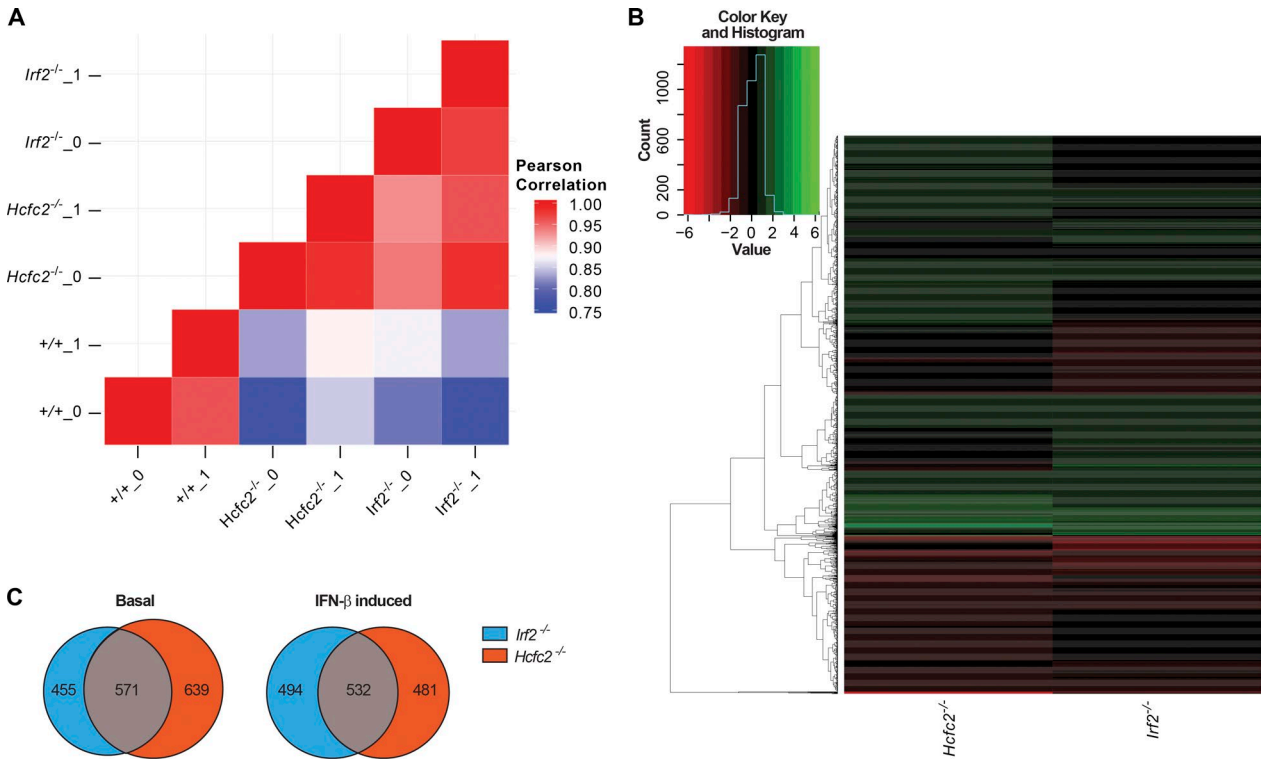

Figure 6. **HCFC2 modulates the expression of numerous IRF2-regulated genes.** Total RNA was isolated from BMDMs from *Irf2*$^{-/-}$ (n = 2), *Hcfc2*$^{-/-}$ (n = 2), and WT (+/+) (n = 2) mice and subjected to RNA-seq analysis. (A) Pearson correlation heat map of the biological replicates. (B) Heat map of the 1,645 differentially expressed genes ($\alpha < 0.05$) between the *Irf2*$^{-/-}$ and *Hcfc2*$^{-/-}$ samples. (C) Venn diagrams indicating the number of genes with significantly changed expression in the *Irf2*$^{-/-}$ and *Hcfc2*$^{-/-}$ mice before and after IFN-β treatment as measured by RNA-seq. Results are representative of two independent experiments.

of DNA, but no direct association between HCFC1 and either DNA or Oct1 was observed (Katan et al., 1990; Kristie and Sharp, 1990; Xiao and Capone, 1990).

By regulating the DNA binding conformation of IRF1 and IRF2, HCFC2 may help these IRFs discriminate between IRF-Es in different genes. Both IRF1 and IRF2 have been shown to distort the conformation of the DNA helix upon binding (Escalante et al., 1998; Fujii et al., 1999), an event that promotes synergistic binding of additional transcriptional regulators; HCFC2 may influence the conformation of IRF1/2-bound DNA. Because IRF2 is an oncogenic protein maintained at low levels in healthy cells (Nguyen et al., 1995), it may rely especially on the support of HCFC2 to stimulate adequate transcription of essential target genes such as *Tlr3*.

In addition to *Tlr3*, numerous genes required both HCFC2 and IRF2 for their normal expression. Among them were a large group of IRGs, which aid in the immune response by, for example, directly inhibiting viral components or activating immune cells (Schneider et al., 2014). Although *Tlr3*$^{-/-}$ mice have been reported to survive as well as or better than WT mice infected with influenza or HSV1, respectively (Zhang et al., 2013), *Hcfc2*$^{fls/fls}$ mice infected with either virus showed significantly reduced survival compared with WT mice. We hypothesize that impaired expression of numerous IRGs, in addition to *Tlr3*, that require HCFC2 for their IRF2-mediated transcription may account for the increased susceptibility of *Hcfc2*$^{fls/fls}$ mice to these viruses. Our data suggest that HCFC2 broadly regulates IRF2-dependent transcription and may therefore be necessary for defense against diverse infections.

MATERIALS AND METHODS

Mice

6-wk- to 6-mo-old male and female mice (*Mus musculus*) on a pure C57BL/6J background were used in experiments. The *Hcfc2*^{fls} (designated *fls*), *Hcfc2*^{min} (designated *min*), and *Hcfc2*^{sca} (designated *sca*) alleles were generated on a pure C57BL/6J background by ENU mutagenesis (Georgel et al., 2008) and are described at http://mutagenetix.utsouthwestern.edu; they are available from the Mutant Mouse Regional Resource Center. *Hcfc2*$^{-/-}$ mice were generated by the TALEN-based method on the C57BL/6J background as described previously (Boch et al., 2009; Moscou and Bogdanove, 2009; Sanjana et al., 2012). The *Irf2*$^{-/-}$ and *MyD88*$^{-/-}$ mice were gifts from Tak Wah Mak (University of Toronto, Toronto, ON, Canada) and Shizuo Akira (Osaka University, Osaka, Japan), respectively. The *Tlr3*$^{-/-}$ mice, *Msr1*$^{-/-}$ mice, and C57BL/10J mice used for positional cloning were purchased from

Table 2. **Genes exhibiting reduced association with IRF2 in ChIP-seq and altered transcript levels in RNA-seq for *Hcfc2*$^{-/-}$ samples relative to WT samples**

Gene name
Genes with lower expression in *Hcfc2*−/− cells
Asah2
Bcl11a
Enpp2
Fam43a
Gca
H2-Q4
Herpud1
Hfe
Ifi44
Rab19
Tlr3
Tnfrsf14
Zbtb18
Genes with higher expression in *Hcfc2*−/− cells
Angpt4
Cald1
Csf1
Has2
Has2os
Hmga2
Inhba
Kirrel3
Mmp27
Mmp20
Msr1
Pdlim1
Pdzrn3
Ptgs2
Rbl1
Sdc2
Sorbs1
Tm4sf1

The Jackson Laboratory. All targeted knockout mice were backcrossed to the C57BL/6J strain for at least six generations. Controls were WT littermates.

All experimental procedures using mice were approved by the Institutional Animal Care and Use Committee of the University of Texas Southwestern Medical Center and were conducted in accordance with institutionally approved protocols and guidelines for animal care and use. Mice were maintained at the University of Texas Southwestern Medical Center, and studies were performed in accordance with institutionally approved protocols. Animals were to be excluded from analysis only if they displayed obvious illness or death (except from HSV1 and influenza infection experiments); these conditions were not observed, and no animals were excluded. No randomization of the allocation of samples or animals to experimental groups was performed.

Positional cloning of *fls*

The index *fls* mutant was outcrossed to C57BL/10J females, and F1 siblings were intercrossed. Bulk segregation analysis was performed as described previously (Xia et al., 2010) using F2 mice grouped into mutant and WT cohorts on the basis of poly(I:C)-induced TNF production. Whole-exome capture from homozygous *fls* mouse tail DNA was performed using the TargetSeq Custom kit (Life Technologies), and exome-enriched DNA was sequenced using an Illumina HiSeq 2500. Sequencing data were analyzed as described previously (Arnold et al., 2011).

Antibodies and reagents

The following antibodies were used: p38 (catalog no. 9212), phosphorylated (p) p38 (catalog no. 4511), ERK (catalog no. 4695), p-ERK (catalog no. 4370), JNK (catalog no. 9252), p-JNK (catalog no. 9251), Akt (catalog no. 4691), p-Akt (catalog no. 4060), p-STAT1 (catalog no. 7649), TBK1 (catalog no. 3504), p-TBK1 (catalog no. 5483), IκB (catalog no. 4814), Tri-Methyl-Histone H3 (Lys4; catalog no. 9751), and GAP DH (catalog no. 8884; Cell Signaling); mouse TLR3 (catalog no. 14-9032-82; eBioscience; STAT1 (catalog no. sc-346), IRF1 (catalog no. sc-497x), IRF2 (catalog no. sc-498x), and HCFC2 (catalog no. sc-367211; Santa Cruz); FLAG tag (catalog no. A8592; Sigma-Aldrich); and Myc tag (catalog no. M047-7), HA tag (catalog no. M180-7), V5 tag (catalog no. M215-7; MBL International).

The following reagents were used: Pam_3CSK_4 and R848 (InvivoGen), poly(I:C) (GE Healthcare), LPS and MALP-2 (ENZO Life Sciences), CpG-ODN 1668 (Sigma-Aldrich), recombinant mouse TNF protein (Life Technologies), mouse TNF ELISA Ready-SET-Go kit (eBioscience), recombinant mouse and human IFN-β (R&D Systems), and mouse IFN-α and IFN-β ELISA kits (PBL Assay Science).

None of the cell lines used (THP1, HEK293T, or NIH-3T3) are listed in the database of commonly misidentified cell lines maintained by the International Cell Line Authentication Committee and National Center for Biotechnology Information Biosample.

PM response assays

Mouse PMs were isolated as previously described (Xiao et al., 2009). In brief, mice of the indicated genotypes were injected i.p. with Brewer's modified thioglycolate (3% wt/vol; BD Biosciences). Macrophages were collected by peritoneal lavage with 5 ml of PBS on day 4 after injection. The PMs were cultured at 37°C in 95% air and 5% CO_2 in DMEM cell culture medium (DMEM containing 10% vol/vol FBS [Gemini Bio Products] and 1% vol/vol penicillin and streptomycin [Life Technologies]).

For TNF and type I IFN production assays, macrophages were preplated onto 96-well plates at a density of 5×10^4 cells/well overnight or for 3 d (specifically for TLR3 signaling). Cells were incubated with varying concentrations of TLR agonists as follows: LPS (125, 250, 500, and 1,000 pg/ml), poly(I:C) (12.5, 25, 50, and 100 μg/ml), Pam_3CSK_4 (12.5, 25, 50, and 100 ng/ml), R848 (2.5, 5, 10, and 20 ng/ml), CpG-ODN 1668 (62.5, 125, 250, and 500 μg/ml), and MALP2 (12.5, 25, 50, and 100 pg/ml), or left unstim-

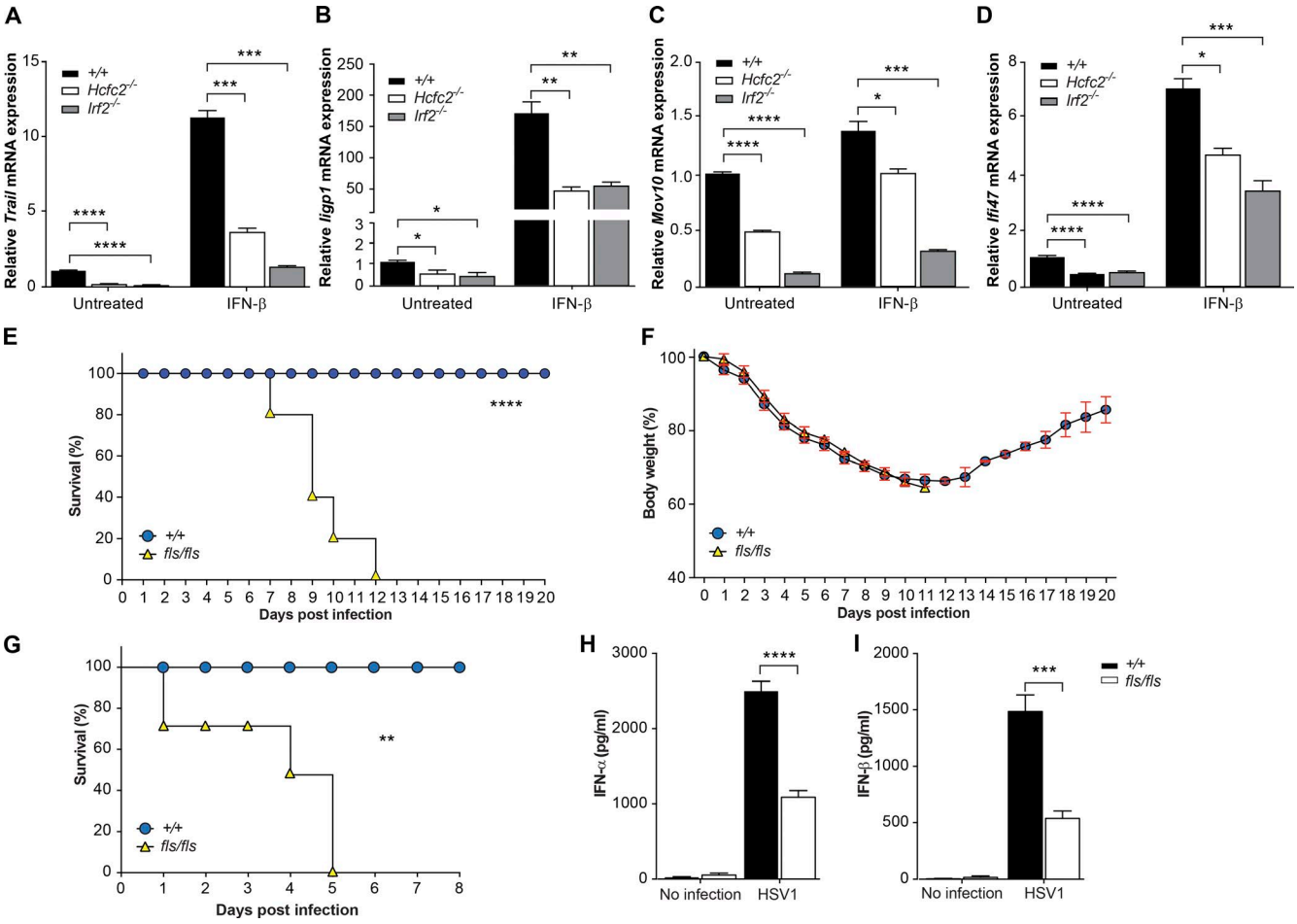

Figure 7. **HCFC2 is required for host defense.** (A–D) qRT-PCR measurement of *Trail* (A), *Iigp1* (B), *Mov10* (C), and *Ifi47* (D) normalized to *Gapdh* in untreated or IFN-β–stimulated BMDMs from $Irf2^{-/-}$, $Hcfc2^{-/-}$, and WT (+/+) mice. (E–I) Homozygous *fls* mice and their WT littermates were challenged with 10^5 pfu IAV per mouse (E and F) or 10^7 pfu HSV1 per mouse (G–I). Kaplan-Meier survival curve (E) and body weight as a percentage of initial body weight after IAV infection (F). Kaplan-Meier survival curve (G) and IFN-α (H) or IFN-β (I) in the serum 4 h after HSV1 infection. *, $P \leq 0.05$; **, $P \leq 0.01$; ***, $P \leq 0.001$; ****, $P \leq 0.0001$, unpaired Student's *t* test (A–D, H, and I), log-rank (Mantel-Cox) test (E and G). Data represent mean ± SEM; $n = 3$ mice (A–D) and $n = 5$ mice per genotype (E–I). Results are representative of three independent experiments.

ulated at 37°C for 4 h. Culture medium was collected for ELISAs. Cells were subjected to an MTT assay (Sigma-Aldrich) for normalization.

For poly(I:C) artificial internalization, macrophages were transfected with DOTAP liposomal transfection reagent (Roche Applied Science) according to the manufacturer's instructions. 24 h later, culture medium was collected for ELISA.

qRT-PCR

Total RNA was extracted and purified with TRIzol reagent (Life Technologies) and reverse-transcribed using SuperScript III First-Strand Synthesis SuperMix (Life Technologies) according to the manufacturer's instructions. Quantitative PCR was performed using the StepOnePlus Real-Time PCR System (Life Technologies). The mRNA levels of the genes of interest were normalized to *Gapdh*, and relative gene expression was calculated using the $2^{-\Delta\Delta Ct}$ method, where $\Delta\Delta Ct = \Delta Ct,\text{sample} - \Delta Ct,\text{reference}$. The following primers were used for qRT-PCR: 5′-TTGTCTTCTGCACGAACCTG-3′, 5′-CGCAACGCAAGGATTTTATT-3′ (*Tlr3*); 5′-AGGATTTCTGGGACTCCACTGA-3′, 5′-TAGAAATGGTGTCCTGAAAGGTTCT-3′ (*Trail*); 5′-CTCTCAGGAGCAGTGAGTGCAT-3′, 5′-GCTGGAGGGCAAATCATTATTC-3′ (*Iigp1*); 5′-AGACCCGTGCCGTTGGT-3′, 5′-GAAGGCTGAGATGAACTGATCCA-3′ (*Ifi47*); 5′-TGGACTGGACCTGGAGACAGA-3′, 5′-GCGATCTTCATTCCATACAGCAT-3′ (*Mov10*); 5′-GGCCCTCTCAGTAAAGTCAGTGA-3′, 5′-GGTGGATACCGTCAACATTCTTAGA-3′ (*Hcfc2*); and 5′-TCATGACCACAGTCCATGCCAT-3′, 5′-GCCTGCTTCACCACCTTCTT-3′ (*Gapdh*).

Immunoprecipitation

293T cells were transfected with the designated expression vectors using PolyJet in vitro DNA transfection reagent (Sig-

naGen). 48 h later, cell lysates were prepared in IPH lysis buffer (50 mM Tris-HCl, pH 8.0, 150 mM NaCl, 5 mM EDTA, and 0.5% NP-40). The lysates were then incubated with magnetic bead–conjugated Myc antibody (MBL International) on a rotator at 4°C overnight. After three washes in cold lysis buffer, proteins bound to the beads were dissociated by boiling in Laemmli SDS sample buffer (Alfa Aesar), separated by SDS-PAGE, and transferred to a membrane. Immunoblotting was performed using the indicated antibodies.

ChIP

ChIP assays were performed as previously reported (Koike et al., 2012; Takahashi et al., 2015). In brief, to prepare chromatin, MEFs were dual cross-linked using 2 nM EGS (20 min) in PBS followed by formaldehyde (1% vol/vol final concentration, 8 min). Dual–cross-linked nuclei were resuspended in 1 ml of lysis buffer (20 mM Tris, pH 8, 150 mM NaCl, 2 mM EDTA, pH 8, 0.1% wt/vol SDS, 1% vol/vol Triton X-100, 1 mM PMSF, and Roche complete EDTA free protease inhibitor cocktail; Whyte et al., 2013) and sonicated nine times for 30 s at 4°C using a Covaris E220 ultrasonicator (150 V peak power, duty factor 10, 200 cycles/burst). 15 µg soluble chromatin was incubated with 1 µg IRF2 antibodies in IP buffer (10 mM Tris, pH 7.5, 150 mM NaCl, 1 mM EDTA, 1% vol/vol Triton X-100, 0.1% wt/vol sodium deoxycholate, 1 mM PMSF, and PI cocktail) overnight at 4°C. 50 µl Dynabeads Protein G was then added and incubated for 2 h at 4°C. After extensive washes, coimmunoprecipitated DNA fragments were eluted, reverse cross-linked, and then purified with the Qiaquick PCR purification kit (QIAGEN). For quantification of coprecipitated DNA, samples were subjected to amplification by using the following primers: 5′-TTTTAA GGGCCTCCTGGGATT-3′, 5′-GGCTCTGAAGCCAGA AACTTACTG-3′ (*Tlr3* IRF-E); 5′-CAGACATGGTAG CTCATATCTTTAATCC-3′, 5′-AGCCATATCTGGCCT GGAAA-3′ (*Tlr3* intron 3); and 5′-CTCCACTCACGG CAAATTCA-3′, 5′-GCCTCACCCCATTTGATGTT-3′ (*Gapdh*). Amplification of *Gapdh* from the unprecipitated chromatin was used to control the amount of input material.

For ChIP-seq, library preparation for next-generation sequencing was based on the Illumina TruSeq ChIP Sample Preparation kit. In brief, ChIP DNA (40 µl) was end-repaired, and ∼150-bp fragments were size-selected using AmpureXP beads followed by adenylation and adapter ligation. After adapter ligation, samples were amplified by PCR and purified with AmpureXP beads and validated on the Agilent 2100 Bioanalyzer. Finally, samples were quantified by Qubit, normalized, and pooled to run on the Illumina NextSeq 500 (high output) using NextSeq 500/550 High Output kit v.2 (150 cycles).

MEF ChIP-seq sample reads from the Illumina NextSeq 500 were mapped to the mm10 genome assembly from the University of California, Santa Cruz, using Bowtie2 v.2.1.0 (Langmead and Salzberg, 2012). Mapped reads containing mapping quality scores >10 were filtered using samtools. Duplicate reads were removed followed by extending the remaining reads to fragment size. Coverage tracks were made by normalizing to 10 million reads. ChIP peaks for MEF samples were identified from uniquely mapped reads without duplicates using MACS (Zhang et al., 2008b) with parameters "-p 1e-5 --gsize mm --nomodel True --wig --space=10" and relevant input chromatin samples as control data. MACS peaks were then subdivided using PeakSplitter with a valley cutoff of 0.7 and were later filtered for summit height >6. To construct a master peak list from the four MEF samples (two *Hcfc2*$^{-/-}$ and two WT), the peaks obtained after PeakSplitter and summit height filtering were merged and compared for overlaps, and the peak with highest summit value was chosen if the summit coordinates were within the fragment size estimate of 192 bp. Raw reads in the master peak regions were quantified using HOMER's (Heinz et al., 2010) annotatePeaks.pl program. The resultant counts matrix was used as input with DESEq2 (Love et al., 2014) and master peak regions with fold change ≥2 and false discovery rate <0.05 were considered differentially enriched and significant. For motif analysis of the 381 IRF2-binding sites (Table S3), binding peak summits ±100 bp were used as input to identify 12-bp motifs using HOMER. HOMER selected a random background sequence with similar GC content to test for statistical significance.

IRF1 and IRF2 DNA-binding activity by gel shift assay and DNA affinity chromatography pulldown

Recombinant FLAG tagged IRF1, IRF2, and HCFC2 were purified with magnetic bead–conjugated FLAG antibody (Sigma-Aldrich) after overexpression in 293T cells. Cell nuclear lysates were prepared with NE-PER Nuclear and Cytoplasmic Extraction Reagents (Thermo Fisher Scientific). Gel shift assays were performed using the LightShift Chemiluminescent EMSA kit (Pierce), according to the manufacturer's instructions. In brief, 1 µg IRF1, 1 µg IRF2, and 0.5 µg HCFC2 recombinant protein or 3 µg nuclear lysate were used in binding reactions, which were further analyzed by electrophoresis through a native 6% polyacrylamide gel. Competitive assays were also performed by addition of 50-fold excess of unlabeled probe at room temperature for 5 min before the addition of the labeled probe. Supershift assays were performed by addition of 2 µg antibodies at room temperature for 15 min after binding reaction. The sequences of the oligonucleotide probes were as follows: mouse *Tlr3* IRF-E sense oligo, biotin-5′-TCAGCCTGAAAGTGAAACTTAAGTTGAG-3′; human *TLR3* IRF-E sense oligo, biotin-5′-AGCTTTACT TTCACTTTCGAGAGTGC-3′ (Heinz et al., 2003).

For DNA affinity chromatography pulldown, 20 fmol biotinylated probe was incubated with 0.5 µg IRF1, 0.5 µg IRF2, and 0.5 µg HCFC2 recombinant protein for 20 min at room temperature in the binding buffer from the LightShift Chemiluminescent EMSA kit supplemented with 2.5% glycerol, 500 ng/µl BSA, and 50 ng/µl poly(dI-dC) competitor. After the incubation, 30 µl streptavidin magnetic beads (New

England Biolabs) were added to the reaction and incubated at 4°C for 1 h. The protein–DNA–streptavidin complex was washed three times with binding buffer and loaded onto an SDS gel. Detection of IRF1, IRF2, and HCFC2 proteins was performed by immunoblotting.

Virus challenge

Age-matched mice (usually 8–12 wk old) were infected with either HSV1 (strain KOS, prepared and provided by the laboratory of Z.J. Chen, University of Texas Southwestern Medical Center, Dallas, TX) at 10^7 pfu per mouse via retro-orbital injection or IAV (strain A/H1N1/CA/2009, prepared and provided by the laboratory of J.-L. Casanova, The Rockefeller University, New York, NY) at 10^5 pfu per mouse via intranasal inoculation. In the HSV1 challenge, the viability of the infected mice was monitored daily for 14 d. 4 h after HSV1 infection, serum was collected and subjected to IFN-α and IFN-β ELISA assays per the manufacturer's instructions. In the IAV challenge, the viability and weight loss were monitored daily for 21 d after inoculation.

High-throughput RNA-seq and bioinformatics analysis

BMDMs were obtained through a macrophage colony–stimulating factor–induced differentiation protocol as previously described (Zhang et al., 2008a). Total RNA was prepared using the RNeasy Plus Mini kit (QIAGEN) according to the manufacturer's instructions. Paired-end 2 × 100 bp sequencing was performed using an Illumina HiSeq 2500. Reads were demultiplexed and converted to fastq format using CASAVA v.1.8.2. Reads were mapped using TopHat2 (http://ccb.jhu.edu/software/tophat/index.shtml; Kim et al., 2013), and differential expression was examined with Cuffdiff, a part of the Cufflinks package (http://cole-trapnell-lab.github.io/cufflinks/; Trapnell et al., 2013). Gene Ontology annotations of differentially expressed genes ($\alpha < 0.05$), between WT and either *Hcfc2*$^{-/-}$ or *Irf2*$^{-/-}$ mice, were annotated using DAVID (the Database for Annotation, Visualization and Integrated Discovery) bioinformatics resources v.6.7 (https://david.ncifcrf.gov; Huang et al., 2007). Heat maps and visualizations were created using the R packages CummeRbund (http://compbio.mit.edu/cummeRbund/), ggplot2 (http://ggplot2.org), and heatmap.2 from gplots (https://mran.microsoft.com/package/gplots/).

Statistical analysis

An unpaired Student's *t* test was used for comparisons between two unpaired experimental groups. For comparisons of differences in responses affected by two factors, two-way ANOVA was used. The log-rank test (Mantel-Cox) was used for comparisons of survival curves. Data represent mean ± SEM in all graphs depicting error bars. The statistical significance of differences between experimental groups was determined using GraphPad Prism v.6. $P < 0.05$ was considered statistically significant. P-values are indicated as follows: *, $P \leq 0.05$; **, $P \leq 0.01$; ***, $P \leq 0.001$; and ****, $P \leq 0.0001$; ns, not significant with $P > 0.05$. No prespecified effect size was assumed, and in general three to five animals or replicates for each genotype or condition were used in experiments; this sample size was sufficient to demonstrate statistically significant differences in comparisons. The investigator was not blinded to genotypes or group allocations during any experiment.

The phenotypic performance of mice (C57BL/6J) and primary cells of these mice is expected to follow a normal distribution, as has been observed in large data sets from numerous phenotypic screens conducted by our group. Variation within each data set obtained by measurements from mice or primary cells was assumed to be similar between genotypes, because all strains were generated and maintained on the same pure inbred background (C57BL/6J); experimental assessment of variance was not performed.

Online supplemental material

Fig. S1 contains the full-size gel and immunoblot images from all figures. Fig. S2 shows the mapping of the interacting domains of IRF2 and HCFC2. Table S1 shows the sequence statistics for ChIP-seq experiments. Table S2 is the master peak list for IRF2 ChIP-seq experiments. Table S3 is the list of 381 differentially enriched master peaks for IRF2 ChIP-seq experiments. Tables S1–S3 are included as Excel files.

ACKNOWLEDGMENTS

The authors thank Peter Jurek for expert assistance with figure preparation.

This work was supported by National Institutes of Health grant U19 AI100627.

The authors declare no competing financial interests.

Author contributions: L. Sun, Z. Jiang, and B. Beutler designed the study. L. Sun, J.H. Choi, J. Wang, K. Wang, V.A. Acosta-Rodriguez, G.K. Kilaru, and J.A. Mohawk performed experiments. L. Sun and Z. Jiang identified and confirmed the *feckless* phenotype. X. Li, M. Tang, and X. Zhan generated the *Hcfc2* knockout mice. J. Quan, L. Scott, and S. Hildebrand performed exon sequencing, RNA sequencing, and data analysis. L. Sun, M. Berger, and X. Du maintained the *feckless* mice. J.S. Takahashi gave suggestions for ChIP analysis. L. Sun, A.R. Murray, D. La Vine, E.M.Y. Moresco, and B. Beutler edited the figures. L. Sun, A.R. Murray, E.M.Y. Moresco, and B. Beutler wrote the manuscript.

Submitted: 27 September 2016

Revised: 13 July 2017

Accepted: 16 August 2017

REFERENCES

Arnold, C.N., Y. Xia, P. Lin, C. Ross, M. Schwander, N.G. Smart, U. Müller, and B. Beutler. 2011. Rapid identification of a disease allele in mouse through whole genome sequencing and bulk segregation analysis. *Genetics.* 187:633–641. https://doi.org/10.1534/genetics.110.124586

Boch, J., H. Scholze, S. Schornack, A. Landgraf, S. Hahn, S. Kay, T. Lahaye, A. Nickstadt, and U. Bonas. 2009. Breaking the code of DNA binding specificity of TAL-type III effectors. *Science.* 326:1509–1512. https://doi.org/10.1126/science.1178811

Childs, K.S., and S. Goodbourn. 2003. Identification of novel co-repressor molecules for Interferon Regulatory Factor-2. *Nucleic Acids Res.* 31:3016–3026. https://doi.org/10.1093/nar/gkg431

Darnell, J.E. Jr., I.M. Kerr, and G.R. Stark. 1994. Jak-STAT pathways and transcriptional activation in response to IFNs and other extracellular signaling proteins. *Science.* 264:1415–1421. https://doi.org/10.1126/science.8197455

DeWitte-Orr, S.J., S.E. Collins, C.M. Bauer, D.M. Bowdish, and K.L. Mossman. 2010. An accessory to the 'Trinity': SR-As are essential pathogen sensors of extracellular dsRNA, mediating entry and leading to subsequent type I IFN responses. *PLoS Pathog.* 6:e1000829. https://doi.org/10.1371/journal.ppat.1000829

Escalante, C.R., J. Yie, D. Thanos, and A.K. Aggarwal. 1998. Structure of IRF-1 with bound DNA reveals determinants of interferon regulation. *Nature.* 391:103–106. https://doi.org/10.1038/34224

Fragale, A., E. Stellacci, R. Ilari, A.L. Remoli, A. Lanciotti, E. Perrotti, I. Shytaj, R. Orsatti, H.R. Lawrence, N.J. Lawrence, et al. 2011. Critical role of IRF-8 in negative regulation of TLR3 expression by Src homology 2 domain-containing protein tyrosine phosphatase-2 activity in human myeloid dendritic cells. *J. Immunol.* 186:1951–1962. https://doi.org/10.4049/jimmunol.1000918

Fujii, Y., T. Shimizu, M. Kusumoto, Y. Kyogoku, T. Taniguchi, and T. Hakoshima. 1999. Crystal structure of an IRF-DNA complex reveals novel DNA recognition and cooperative binding to a tandem repeat of core sequences. *EMBO J.* 18:5028–5041. https://doi.org/10.1093/emboj/18.18.5028

Garcia-Cattaneo, A., F.X. Gobert, M. Müller, F. Toscano, M. Flores, A. Lescure, E. Del Nery, and P. Benaroch. 2012. Cleavage of Toll-like receptor 3 by cathepsins B and H is essential for signaling. *Proc. Natl. Acad. Sci. USA.* 109:9053–9058. https://doi.org/10.1073/pnas.1115091109

Georgel, P., X. Du, K. Hoebe, and B. Beutler. 2008. ENU mutagenesis in mice. *Methods Mol. Biol.* 415:1–16.

Gerster, T., and R.G. Roeder. 1988. A herpesvirus trans-activating protein interacts with transcription factor OTF-1 and other cellular proteins. *Proc. Natl. Acad. Sci. USA.* 85:6347–6351. https://doi.org/10.1073/pnas.85.17.6347

Hardarson, H.S., J.S. Baker, Z. Yang, E. Purevjav, C.H. Huang, L. Alexopoulou, N. Li, R.A. Flavell, N.E. Bowles, and J.G. Vallejo. 2007. Toll-like receptor 3 is an essential component of the innate stress response in virus-induced cardiac injury. *Am. J. Physiol. Heart Circ. Physiol.* 292:H251–H258. https://doi.org/10.1152/ajpheart.00398.2006

Heinz, S., V. Haehnel, M. Karaghiosoff, L. Schwarzfischer, M. Müller, S.W. Krause, and M. Rehli. 2003. Species-specific regulation of Toll-like receptor 3 genes in men and mice. *J. Biol. Chem.* 278:21502–21509. https://doi.org/10.1074/jbc.M301476200

Heinz, S., C. Benner, N. Spann, E. Bertolino, Y.C. Lin, P. Laslo, J.X. Cheng, C. Murre, H. Singh, and C.K. Glass. 2010. Simple combinations of lineage-determining transcription factors prime cis-regulatory elements required for macrophage and B cell identities. *Mol. Cell.* 38:576–589. https://doi.org/10.1016/j.molcel.2010.05.004

Huang, D.W., B.T. Sherman, Q. Tan, J.R. Collins, W.G. Alvord, J. Roayaei, R. Stephens, M.W. Baseler, H.C. Lane, and R.A. Lempicki. 2007. The DAVID Gene Functional Classification Tool: a novel biological module-centric algorithm to functionally analyze large gene lists. *Genome Biol.* 8:R183. https://doi.org/10.1186/gb-2007-8-9-r183

Ivashkiv, L.B., and L.T. Donlin. 2014. Regulation of type I interferon responses. *Nat. Rev. Immunol.* 14:36–49. https://doi.org/10.1038/nri3581

Karimi-Googheri, M., and M.K. Arababadi. 2014. TLR3 plays significant roles against hepatitis B virus. *Mol. Biol. Rep.* 41:3279–3286. https://doi.org/10.1007/s11033-014-3190-x

Katan, M., A. Haigh, C.P. Verrijzer, P.C. van der Vliet, and P. O'Hare. 1990. Characterization of a cellular factor which interacts functionally with Oct-1 in the assembly of a multicomponent transcription complex. *Nucleic Acids Res.* 18:6871–6880. https://doi.org/10.1093/nar/18.23.6871

Kim, D., G. Pertea, C. Trapnell, H. Pimentel, R. Kelley, and S.L. Salzberg. 2013. TopHat2: accurate alignment of transcriptomes in the presence of insertions, deletions and gene fusions. *Genome Biol.* 14:R36. https://doi.org/10.1186/gb-2013-14-4-r36

Koike, N., S.H. Yoo, H.C. Huang, V. Kumar, C. Lee, T.K. Kim, and J.S. Takahashi. 2012. Transcriptional architecture and chromatin landscape of the core circadian clock in mammals. *Science.* 338:349–354. https://doi.org/10.1126/science.1226339

Kristie, T.M., and P.A. Sharp. 1990. Interactions of the Oct-1 POU subdomains with specific DNA sequences and with the HSV alpha-trans-activator protein. *Genes Dev.* 4(12b):2383–2396. https://doi.org/10.1101/gad.4.12b.2383

Kristie, T.M., J.L. Pomerantz, T.C. Twomey, S.A. Parent, and P.A. Sharp. 1995. The cellular C1 factor of the herpes simplex virus enhancer complex is a family of polypeptides. *J. Biol. Chem.* 270:4387–4394. https://doi.org/10.1074/jbc.270.9.4387

Langmead, B., and S.L. Salzberg. 2012. Fast gapped-read alignment with Bowtie 2. *Nat. Methods.* 9:357–359. https://doi.org/10.1038/nmeth.1923

Le Goffic, R., V. Balloy, M. Lagranderie, L. Alexopoulou, N. Escriou, R. Flavell, M. Chignard, and M. Si-Tahar. 2006. Detrimental contribution of the Toll-like receptor (TLR)3 to influenza A virus-induced acute pneumonia. *PLoS Pathog.* 2:e53. https://doi.org/10.1371/journal.ppat.0020053

Leung, Y.H., J.M. Nicholls, C.K. Ho, S.F. Sia, C.K. Mok, S.A. Valkenburg, P. Cheung, K.P. Hui, R.W. Chan, Y. Guan, et al. 2014. Highly pathogenic avian influenza A H5N1 and pandemic H1N1 virus infections have different phenotypes in Toll-like receptor 3 knockout mice. *J. Gen. Virol.* 95:1870–1879. https://doi.org/10.1099/vir.0.066258-0

Limmon, G.V., M. Arredouani, K.L. McCann, R.A. Corn Minor, L. Kobzik, and F. Imani. 2008. Scavenger receptor class-A is a novel cell surface receptor for double-stranded RNA. *FASEB J.* 22:159–167. https://doi.org/10.1096/fj.07-8348com

Love, M.I., W. Huber, and S. Anders. 2014. Moderated estimation of fold change and dispersion for RNA-seq data with DESeq2. *Genome Biol.* 15:550. https://doi.org/10.1186/s13059-014-0550-8

Marsden, H.S., M.E. Campbell, L. Haarr, M.C. Frame, D.S. Parris, M. Murphy, R.G. Hope, M.T. Muller, and C.M. Preston. 1987. The 65,000-Mr DNA-binding and virion trans-inducing proteins of herpes simplex virus type 1. *J. Virol.* 61:2428–2437.

McCartney, S.A., W. Vermi, S. Lonardi, C. Rossini, K. Otero, B. Calderon, S. Gilfillan, M.S. Diamond, E.R. Unanue, and M. Colonna. 2011. RNA sensor-induced type I IFN prevents diabetes caused by a β cell-tropic virus in mice. *J. Clin. Invest.* 121:1497–1507. https://doi.org/10.1172/JCI44005

Moscou, M.J., and A.J. Bogdanove. 2009. A simple cipher governs DNA recognition by TAL effectors. *Science.* 326:1501. https://doi.org/10.1126/science.1178817

Nguyen, H., A. Mustafa, J. Hiscott, and R. Lin. 1995. Transcription factor IRF-2 exerts its oncogenic phenotype through the DNA binding/transcription repression domain. *Oncogene.* 11:537–544.

Nhu, Q.M., N. Cuesta, and S.N. Vogel. 2006. Transcriptional regulation of lipopolysaccharide (LPS)-induced Toll-like receptor (TLR) expression in murine macrophages: role of interferon regulatory factors 1 (IRF-1) and 2 (IRF-2). *J. Endotoxin Res.* 12:285–295. https://doi.org/10.1177/09680519060120050401

Prakash, K., and P.C. Rath. 2010. Replacement of the C-terminal tetrapeptide (314 PAPV 317 to 314 SSSM 317) in interferon regulatory factor-2 alters its N-terminal DNA-binding activity. *J. Biosci.* 35:547–556. https://doi.org/10.1007/s12038-010-0063-x

Qi, R., D. Singh, and C.C. Kao. 2012. Proteolytic processing regulates Toll-like receptor 3 stability and endosomal localization. *J. Biol. Chem.* 287:32617–32629. https://doi.org/10.1074/jbc.M112.387803

Ren, G., K. Cui, Z. Zhang, and K. Zhao. 2015. Division of labor between IRF1 and IRF2 in regulating different stages of transcriptional activation in cellular antiviral activities. *Cell Biosci.* 5:17. https://doi.org/10.1186/s13578-015-0007-0

Rudd, B.D., E. Burstein, C.S. Duckett, X. Li, and N.W. Lukacs. 2005. Differential role for TLR3 in respiratory syncytial virus-induced chemokine expression. *J. Virol.* 79:3350–3357. https://doi.org/10.1128/JVI.79.6.3350-3357.2005

Sanjana, N.E., L. Cong, Y. Zhou, M.M. Cunniff, G. Feng, and F. Zhang. 2012. A transcription activator-like effector toolbox for genome engineering. *Nat. Protoc.* 7:171–192. https://doi.org/10.1038/nprot.2011.431

Sarkar, S.N., K.L. Peters, C.P. Elco, S. Sakamoto, S. Pal, and G.C. Sen. 2004. Novel roles of TLR3 tyrosine phosphorylation and PI3 kinase in double-stranded RNA signaling. *Nat. Struct. Mol. Biol.* 11:1060–1067. https://doi.org/10.1038/nsmb847

Schneider, W.M., M.D. Chevillotte, and C.M. Rice. 2014. Interferon-stimulated genes: a complex web of host defenses. *Annu. Rev. Immunol.* 32:513–545. https://doi.org/10.1146/annurev-immunol-032713-120231

Stark, G.R., I.M. Kerr, B.R. Williams, R.H. Silverman, and R.D. Schreiber. 1998. How cells respond to interferons. *Annu. Rev. Biochem.* 67:227–264. https://doi.org/10.1146/annurev.biochem.67.1.227

Takahashi, J.S., V. Kumar, P. Nakashe, N. Koike, H.C. Huang, C.B. Green, and T.K. Kim. 2015. ChIP-seq and RNA-seq methods to study circadian control of transcription in mammals. *Methods Enzymol.* 551:285–321. https://doi.org/10.1016/bs.mie.2014.10.059

Toscano, F., Y. Estornes, F. Virard, A. Garcia-Cattaneo, A. Pierrot, B. Vanbervliet, M. Bonnin, M.J. Ciancanelli, S.Y. Zhang, K. Funami, et al. 2013. Cleaved/associated TLR3 represents the primary form of the signaling receptor. *J. Immunol.* 190:764–773. https://doi.org/10.4049/jimmunol.1202173

Trapnell, C., D.G. Hendrickson, M. Sauvageau, L. Goff, J.L. Rinn, and L. Pachter. 2013. Differential analysis of gene regulation at transcript resolution with RNA-seq. *Nat. Biotechnol.* 31:46–53. https://doi.org/10.1038/nbt.2450

Whyte, W.A., D.A. Orlando, D. Hnisz, B.J. Abraham, C.Y. Lin, M.H. Kagey, P.B. Rahl, T.I. Lee, and R.A. Young. 2013. Master transcription factors and mediator establish super-enhancers at key cell identity genes. *Cell.* 153:307–319. https://doi.org/10.1016/j.cell.2013.03.035

Wysocka, J., and W. Herr. 2003. The herpes simplex virus VP16-induced complex: the makings of a regulatory switch. *Trends Biochem. Sci.* 28:294–304. https://doi.org/10.1016/S0968-0004(03)00088-4

Xia, Y., S. Won, X. Du, P. Lin, C. Ross, D. La Vine, S. Wiltshire, G. Leiva, S.M. Vidal, B. Whittle, et al. 2010. Bulk segregation mapping of mutations in closely related strains of mice. *Genetics.* 186:1139–1146. https://doi.org/10.1534/genetics.110.121160

Xiao, P., and J.P. Capone. 1990. A cellular factor binds to the herpes simplex virus type 1 transactivator Vmw65 and is required for Vmw65-dependent protein-DNA complex assembly with Oct-1. *Mol. Cell. Biol.* 10:4974–4977. https://doi.org/10.1128/MCB.10.9.4974

Xiao, N., C. Eidenschenk, P. Krebs, K. Brandl, A.L. Blasius, Y. Xia, K. Khovananth, N.G. Smart, and B. Beutler. 2009. The Tpl2 mutation Sluggish impairs type I IFN production and increases susceptibility to group B streptococcal disease. *J. Immunol.* 183:7975–7983. https://doi.org/10.4049/jimmunol.0902718

Yamamoto, M., S. Sato, K. Mori, K. Hoshino, O. Takeuchi, K. Takeda, and S. Akira. 2002. Cutting edge: a novel Toll/IL-1 receptor domain-containing adapter that preferentially activates the IFN-beta promoter in the Toll-like receptor signaling. *J. Immunol.* 169:6668–6672. https://doi.org/10.4049/jimmunol.169.12.6668

Zhang, S.Y., E. Jouanguy, S. Ugolini, A. Smahi, G. Elain, P. Romero, D. Segal, V. Sancho-Shimizu, L. Lorenzo, A. Puel, et al. 2007. TLR3 deficiency in patients with herpes simplex encephalitis. *Science.* 317:1522–1527. https://doi.org/10.1126/science.1139522

Zhang, S.Y., M. Herman, M.J. Ciancanelli, R. Pérez de Diego, V. Sancho-Shimizu, L. Abel, and J.L. Casanova. 2013. TLR3 immunity to infection in mice and humans. *Curr. Opin. Immunol.* 25:19–33. https://doi.org/10.1016/j.coi.2012.11.001

Zhang, X., R. Goncalves, and D.M. Mosser. 2008a. The isolation and characterization of murine macrophages. *Curr. Protoc. Immunol.* Chapter 14:Unit 14.1. https://doi.org/10.1002/0471142735.im1401s83

Zhang, Y., T. Liu, C.A. Meyer, J. Eeckhoute, D.S. Johnson, B.E. Bernstein, C. Nusbaum, R.M. Myers, M. Brown, W. Li, and X.S. Liu. 2008b. Model-based analysis of ChIP-Seq (MACS). *Genome Biol.* 9:R137. https://doi.org/10.1186/gb-2008-9-9-r137